Prediction of High-Resolution Flowfields for Rotorcraft Aeroacoustics

Todd R. Quackenbush*
Continuum Dynamics, Inc., Princeton, New Jersey 08543
and
Donald B. Bliss†
Duke University, Durham, North Carolina 27705

The prediction of noise due to the impingement of the main-rotor wake of a helicopter on the tail rotor and other main-rotor blades requires the efficient computation of the wake-induced velocity field. This paper describes the development of a new treatment of the vortex wake of a helicopter that permits highly accurate resolution of the flowfield experienced by the tail rotor with modest computational effort relative to alternative models. The new approach incorporates an advanced full-span free wake model of the main rotor in a scheme that reconstructs high-resolution flow solutions from preliminary, computationally inexpensive simulations with coarse resolution. The heart of the reconstruction procedure is a novel method for using local velocity correction terms to capture the steep velocity gradients characteristic of the vortex-dominated incident flow. Sample calculations have been undertaken to examine the principal types of interactions between the tail rotor and the main-rotor wake and to examine the performance of the new method. The results confirm the success of this approach in capturing the high-resolution flows necessary for analysis of rotor-wake/rotor interactions with dramatically reduced computational cost. The steps required for the extension of this method to studies of more general classes of interactions are also discussed.

Nomenclature

b	= semispan of a parabolic vortex element
C_T	= rotor thrust coefficient
i,j,k	= unit vectors in the parabolic element coordinate system
$q_{(\,)}$	= induced velocity
R	= main-rotor radius
r_c	= physical vortex core radius
r_f	= artificial ("fat") vortex core radius
r_m	= minimum distance from filament to evaluation point
r_v	= vector from parabolic vortex element to evaluation point
U,V,W	= wake-induced velocity in gobal X,Y,Z directions
U_∞	= freestream velocity component in X direction
v	= vortex swirl velocity
W_∞	= freestream velocity component in Z direction
X,Y,Z	= global position coordinates in the shaft reference frame
X_{TR},Y_{TR},Z_{TR}	= local position coordinates in the tail-rotor reference frame
x,y,z	= local position coordinates on a parabolic element
ϵ	= parabolic arc curvature parameter
Γ	= vortex filament circulation
μ	= rotor advance ratio, $U_\infty/\Omega R$
ρ	= local filament radius of curvature
Ψ	= azimuth angle of reference rotor blade
Ω	= main-rotor angular velocity

Received Dec. 11, 1989; revision received July 25, 1990; accepted for publication Aug. 26, 1990.

*Senior Associate. Senior Member AIAA.
†Associate Professor, Member AIAA.

Introduction

THE principal objective of this effort was to demonstrate the feasibility of developing an efficient and accurate Lagrangian simulation of the unsteady vorticity field in the vicinity of a helicopter main rotor that could serve as the foundation for an analysis of the noise generated by main-rotor/tail-rotor interactions. This work represents the first step in an effort to produce an analysis capable of addressing broad classes of rotor-wake/rotor phenomena and emphasizes those that figure in main-rotor/tail-rotor interactions. It is important to note at the outset that the techniques developed here are applicable to the analysis of the helicopter main rotors, though the focus of the present paper is on tail-rotor applications. Part of the charter of the preliminary study discussed here was to identify the enhancements and modifications that would be required to produce a general analysis in follow-on work, and the conclusions reached on this topic are outlined in the summary.

For several years, it has been clearly recognized that the generation of noise from main-rotor/tail-rotor interactions poses one of the most difficult challenges in the effort to reduce the noise of single-rotor helicopters. It is known that the origin of much of the subjectively objectionable discrete frequency noise lies in the "cutting" of the main-rotor vortex wake by the tail rotor. The impulsive nature of such interactions and the high-velocity gradients experienced by the tail-rotor blades during the interaction lead to strong acoustic emissions at a large number of harmonics of tail-rotor blade passage frequency.

Substantial effort has gone into both experimental and analytical study of these issues in recent years (e.g., Refs. 1–6), and this work has yielded considerable insight into main-rotor/tail-rotor interaction noise, though many issues remain to be addressed. Other recent work in the study of rotor-wake vortex dynamics has provided the means to overcome some of the limitations of previous analyses. As discussed in Refs. 7–11, application of a new vortex wake dynamics analysis method using curved vortex elements has led to a substantial improvement in the prediction of main-rotor blade higher harmonic airloading. The effort discussed here (and at greater

length in Ref. 12) focused on incorporating an advanced free-wake model in an analysis of the tail-rotor flowfield designed for application to the problem of predicting tail-rotor noise due to interaction with the main rotor.

The ultimate goal of this effort is to develop an aeroacoustic analysis for general wake/rotor interactions, and the tail-rotor problem was judged to be a reasonable starting point. Any such general analysis, of course, must incorporate a number of key features. First, it must define the geometry and strength of the main-rotor wake in a realistic fashion so that the induced velocity field in the vicinity of the tail rotor may be predicted accurately and without prohibitive computational effort. Second, the simulation must be able to reliably define the flight regimes where significant main-rotor/tail-rotor interactions occur, and it must accurately capture the types of interactions (e.g., the filament intersection geometry) that take place. Third, the simulation should include an appropriate treatment of the unsteady aerodynamic loads on the rotor and should properly account for the complex spatial and temporal variation in these loads and the consequent far field noise. This present effort centered on the first two topics, and, in particular, on demonstrating the capabilities of a new high-resolution flowfield analysis for the tail rotor. The results to be presented below include the solution of model problems demonstrating the success of a new approach to the analysis of tail-rotor flowfields, an approach that can obtain refined spatial and temporal resolution of the incident velocity field with a dramatic reduction in computational effort relative to alternative models. These results will be presented following a discussion of some of the fundamental aspects of the new methods developed here.

To analyze the loads on the tail rotor in the presence of the main-rotor wake, it is necessary to accurately model the effect of the vortex wake of the main rotor. Over the past 20 years, a variety of rotor-wake models have been developed, largely for application to problems concerning isolated main-rotor performance and airloads.[13-15] These earlier models usually employed a single free tip vortex, with relatively simple models of the inboard wake. In many important forward flight conditions, though, (particularly at high speed) the rotor-wake structure can become very complicated, and the simple tip vortex representation often used in the past is inadequate. The new wake analysis methods described in Ref. 9–11 seek to represent the important features of the resulting wake generated along the full span of the blade. Figure 1 shows the wake geometry calculated by this new full-span free-wake method for one blade of a four-bladed rotor at advance ratio 0.39. An examination of Fig. 1 shows that the advancing side wake is in some cases a complicated structure with considerable distributed vorticity, not a simple rolled-up tip vortex as has often been assumed. The looping (or connecting) between outboard and inboard filaments is associated with changes in the maximum bound circulation on the blade. A strong root vortex structure is also evident. The actual aerodynamic environment experienced by the regions immersed in this complex wake structure can also be inferred from Fig. 1. From the standpoint of the flow in the vicinity of the tail rotor, this plot shows a remarkably complicated incident wake structure.

The curved vortex elements used to represent vortex filaments in Fig. 1 are laid down along contours of constant sheet strength in the wake. The vortex filaments leaving the blade are all of constant vortex sheet strength, and each one is of equal value. For this reason, close spacing between filaments implies a strong net influence from that region of the wake, whereas, a sparse spacing indicates a region of little influence. Thus, this model provides a visually meaningful representation of the wake since the filaments correspond to the actual resultant vorticity field. Also, the skewed/curved filaments provide a natural representation of the free-wake vorticity field, which simultaneously accounts for both shed and trailed vorticity. Since a single resultant curved element, on the average, can replace two perpendicular straight segments, this

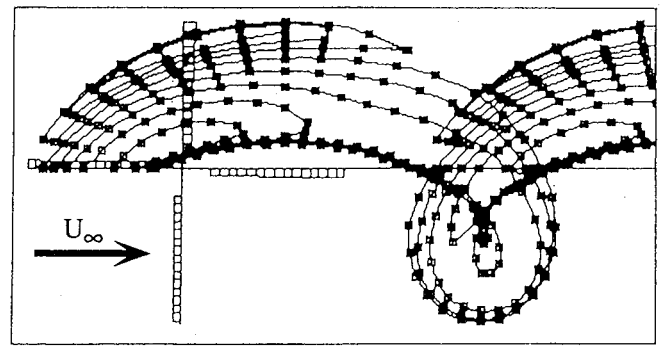

Fig. 1 Top view of the wake geometry of one blade of a four-bladed rotor at advance ratio 0.39. (Boxes indicate collocation points defining the filaments.)

model represents a more efficient approach to free wake modeling. Though the full-span wake features significant efficiencies relative to previous free-wake models, it is still a Lagrangian treatment of the vorticity field, and thus large amounts of computation time are usually required to resolve the rapid spatial and temporal variations in the flowfield required for rotor aeroacoustics. To alleviate this problem, a new framework for the execution of free-wake calculations was developed here, one which permits accurate resolution of the steep velocity gradients associated with vortex-dominated flowfields with a small fraction of the computer time usually required.

Development of an Efficient High-Resolution Flowfield Analysis

Given the full-span wake model just described, it is a straightforward matter in principle to compute the time-varying inflow at the tail rotor due to main-rotor wake. The main-rotor simulation should be run with sufficiently small time steps to provide the time history of inflow needed at the tail-rotor blades to predict the aerodynamic load on the blades. Recall that in Lagrangian rotor-wake calculations, each time step corresponds to one increment in rotor azimuth. The frequency content of experimental measurements of the rotor acoustic output in studies such as Refs. 2, 4, and 16 indicate that airloads up to at least 30–50 harmonics of the rotor rotation rate must be resolved. This means that as many as several hundred time steps per main-rotor revolution may be required to provide sufficient frequency resolution. The use of such refined time steps presents nearly insurmountable computational obstacles to Lagrangian free-wake models, since the computation time required to update the wake at each step in the simulation is proportional to the square of the number of vortex elements used to model each turn of wake (which, in a Lagrangian calculation, equals the number of time steps in each rotor revolution).

The first step in motivating a new approach is to appreciate that the rapid temporal variations in the velocity field (and airloads) observed on the tail rotor are intimately related to the steep spatial velocity gradients experienced by the tail-rotor blades as they encounter the vortex wake of the main rotor. As the blades cut the main rotor tip vortices (whose core size is typically much less than the tail-rotor radius, though generally of the same order as the blade chord), the relative motion of the blades and the vortices sets up rapidly varying loads that produce the "harmonic" noise characteristic of main-rotor/tail-rotor interaction. Because the spatial velocity gradients are so large, the points on the tail-rotor disk where the velocity is evaluated must be very densely spaced to ensure adequate resolution. Since these evaluation points are typically located on the tail-rotor blades themselves (whose position is changing continuously during the calculation), this is equivalent to requiring very small time steps in the calculation. A method that could accurately and efficiently resolve the effect of these steep spatial gradients would also translate into

a way to obtain good temporal resolution without excessive computational penalty.

Assume, for example, that the core size of the main-rotor vortices penetrating the tail-rotor disk could be increased arbitrarily. This would make the velocity gradients encountered by the tail-rotor blades much smoother and, consequently, far fewer steps would be required to resolve the blade loads to an acceptable degree of accuracy since the required spatial density of evaluation points would be reduced. A simulation with artificially "fat" vortex cores, then, could be undertaken with current methods using reasonable amounts of CPU time, even though the solution would be physically meaningless. However, if the use of the fat core was restricted to computation of the induced velocity on the tail-rotor disk itself and the actual vortex core was used elsewhere, then it would be true that the fat core solution correctly captured the contributions of the far field to the flow solution at the disk itself. Any errors due to the use of the fat core would be due to local effects, and it would be possible to correct the solution locally to recover the physically correct solution with the actual core.

The fundamental approach developed here to obtain refined time histories of tail-rotor inflow can be described as follows. First, the basic full-span, multiple-filament free-wake model of the main rotor is run for a specified number of main-rotor revolutions with the artificial, fat vortex core in place for computation of the velocities in the tail-rotor disk. Typical simulations are done with relatively coarse time steps, with typical choices of between 12 and 32 steps per main-rotor revolution; this is far fewer than the number of azimuthal increments normally required for resolution of acoustic events. At each time step a "snapshot" of the flowfield generated at specified points on the tail-rotor disk is computed and stored. Simultaneously, the positions of vortex filament intersections with the tail-rotor disk are recorded, as are the filament orientations at these points. This completes the initial (and by far the most computationally intensive) phase of the analysis.

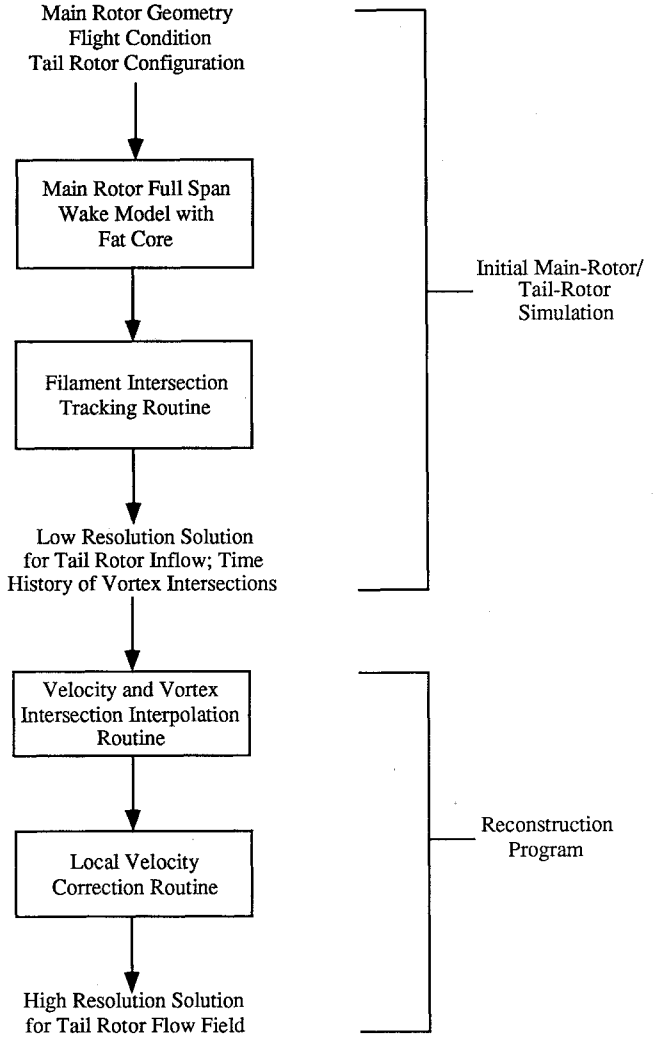

Fig. 2 Flow chart for the analysis of high-resolution tail-rotor inflow.

Once this portion of the simulation is completed, it becomes the task of a reconstruction program to take the stored information on the wake-induced velocity field and the "tracks" of the vortex intersections with the tail-rotor disk and regenerate the velocity field induced by the transit of the actual wake vortices across the disk. This is accomplished by first interpolating the smoothed-out velocity field generated by using the fat core to yield the "background" flow at each of the evaluation points in the rotor disk. Note that this is interpolation in time, which can be carried out in confidence because the use of the fat core has eliminated the steep velocity gradients from the velocity field around the disk. Second, the positions of the vortex intersections with the disk are also interpolated to set up the information needed for producing flow histories with high temporal resolution. By applying appropriate local correction terms to the background flow computed using the fat core, the velocity induced using the actual vortex core can be recaptured while simultaneously refining the time history of the flowfield at the tail rotor.

The structure of the programs that embody this new approach is shown in Fig. 2. As will be discussed below, with the current analysis interpolation of as many as five time increments between the relatively coarse time steps used in the initial free-wake calculation has been achieved, and the use of finer time increments is almost certainly possible. The ratio of the time required by the new approach to that required by a traditional Lagrangian analysis varies essentially as the cube of temporal multiplier for initial value problems. This means that an interpolation multiplier of two leads to a factor of eight saving in CPU time, while 5 leads to a factor of 125 and 10 to a factor of 1000. (This takes advantage of the fact that the reconstruction program requires a negligibly small amount of CPU time). Thus, this new approach brings the temporal resolution required for tail-rotor aeroacoustic analyses within reach while retaining the refined, full-span model of the incident main-rotor wake.

One of the critical elements in this approach is the procedure for finding the velocity correction terms for filament interactions with the tail-rotor disk. The formulation of the local correction terms involves computing the induced velocity contributions of individual filaments at points on the tail-rotor disk with an assumed vortex core size—the fat vortex core—as opposed to the actual, physically correct core size. An analytical solution is then computed based on the near-field filament configuration incorporating the local position and curvature of the filament modeled as a parabolic arc. Actually, two such analytical solutions are superimposed. One solution adds the contribution of a vortex filament with a physically realistic core, and the other solution subtracts a vortex filament with the same fat core used in the numerical calculation. The net effect in the near field is to cancel the numerical fat core effect and add the effect of the actual core size. At the same time, the far field effect remains unchanged since the two portions of the analytical solution cancel in the far field. Once the vortex filament trajectories have been obtained from the numerical free-wake calculation, the addition of the analytical correction is a very efficient way to perform a high-resolution calculation of velocity field at the tail-rotor disk.

Since the free-wake analysis treats each vortex filament as having an artificially large vortex core when calculating the tail-rotor velocity field, this initial phase of the simulation produces a low-resolution numerical solution for the velocity field at the tail-rotor disk. The velocity calculated in the tail-

rotor plane has gradients smoothed to a length scale no smaller than the order of the fat core size. The actual choice of core size for the artificial fat core is dictated by a number of factors in the calculation, such as time step, vortex element length, etc., but in all cases the core size must be at least as large as the spacing between evaluation points on the tail-rotor disk. This criterion assures a meaningful degree of smoothing so that the smoothed velocity field can adequately captured by the limited number of evaluation points on the tail-rotor disk. Based on work with similar calculations involving vortex/surface interactions (Ref. 17), it was judged appropriate to use fat cores three to four times the size of the physical core.

The numerical smoothing is achieved by use of a particular vortex core model chosen for its ease of implementation, smooth behavior, and is functional simplicity. The latter is important for the analytical near-field solution discussed below. This particular swirl velocity distribution has also achieved wide use as a core model in rotary wing applications (see Ref. 14). In its two-dimensional form, the vortex swirl velocity is expressed as

$$v = \frac{\Gamma}{2\pi} \frac{r}{r^2 + r_c^2} \tag{1}$$

where Γ is the circulation, r the radius from the center of the vortex, and r_c the radial length scale of the core. For small r ($\ll r_c$) the velocity behaves as if in solid body rotation, whereas, for large r ($\gg r_c$) the velocity behaves as an irrotational point vortex. The swirl velocity reaches a maximum value at $r = r_c$. The corresponding functional form has been imposed on the swirl velocity expression for the curved vortex elements used in the free-wake code. During the initial free-wake calculation, velocities are evaluated on the tail-rotor disk using r_f in place of r_c, where r_f is a fat core radius that provides smoothing in this phase of the computation. For all other velocity calculations (e.g., wake-on-wake calculations that determine vortex trajectories), a physically realistic value of core radius r_c is used. Note that $r_f \gg r_c$.

The high-resolution analytical solution that is applied after this initial calculation is designed to correct the velocity field locally to achieve high accuracy in the tail-rotor plane. This solution is obtained by integrating the Biot-Savart law along a centered parabolic filament with the core velocity distribution discussed earlier. The resulting expression is used twice: once with the core radius equal to r_f and once with the radius equal to r_c. The parabolic arc used in the analytical correction is positioned at a point along the actual filament that is the minimum distance from the point of evaluation, and the arc is therefore centered with respect to this point. The orientation and local radius of curvature of the parabolic arc are chosen to have it coincide locally with the actual vortex filament. Using this configuration, the arc solution is used to cancel the local numerical smoothing effect by using the same fat core size r_f with the opposite sign of circulation. The correct answer for the physically realistic core size is then obtained by adding an arc with the correct sign circulation and the correct core size r_c. The superposition of these solutions is shown schematically in Fig. 3.

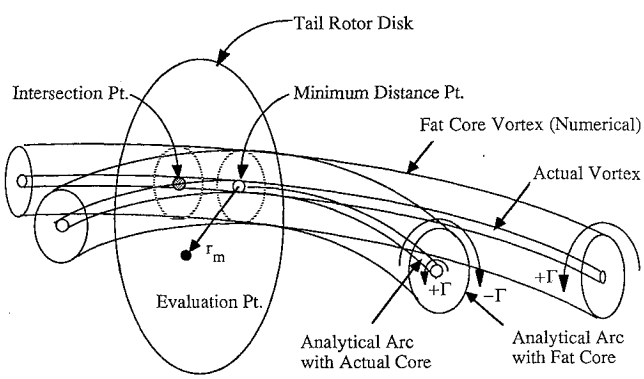

Fig. 3 Sketch showing the method of superimposing local analytical arc solutions on the low-resolution numerical solution to obtain a high-resolution result.

The addition of the numerical fat core solution, the analytical real core solution, and the opposite sign analytical fat core solution together form a composite solution in much the same sense of the method of matched asymptotic expansions. At the nearest points along the filament, the fat core numerical and analytical solutions cancel leaving the analytical actual core solution. The shape of the parabolic filament corresponds well with the actual filament in this region. At points farther out along the arc, where the point of evaluation falls outside the fat core radius, the two opposite sign analytical solutions cancel each other. In this region the numerical fat core result, which has the correct far field shape, gives an accurate answer since the core size has no effect. By analogy to the method of matched asymptotic expansions, the fat core numerical solution is like the outer solution and the actual core analytical solution is like the inner solution. The analytical fat core solution is like the outer limit of the inner solution, or alternatively like the inner limit of the outer solution. In matched asymptotic expansions, the uniformly valid composite solution is the outer solution plus the inner solution minus the outer limit of the inner solution (or the inner limit of the outer solution). The composite solution for the present approach is formed in exactly the same way. The result of this superposition of solutions is a relatively simple expression for the velocity correction term as a function of the orientation of the filament, its position relative to the point of evaluation, and the core size. This development is described in detail in Ref. 12, though the major points can be summarized as follows.

As noted previously, the local analytical solution is based on the velocity field of a parabolic arc. The geometry for the analytical calculation for this centered arc is shown in Fig. 4, and this figure serves to define the important parameters of the arc calculation. The Biot-Savart law, modified to include the vortex core effect, has the form

$$q = -\frac{\Gamma}{2\pi} \int_{\text{arc}} \frac{r_v \times ds}{\left[r_v^2 + r_c^3\right]^{3/2}} \tag{2}$$

where r_v is the distance from a point on the filament to the point of evaluation. The parabolic arc is described by the expression $y = \epsilon x^2$. The parameter $\epsilon = -1/2\rho$, where ρ is the

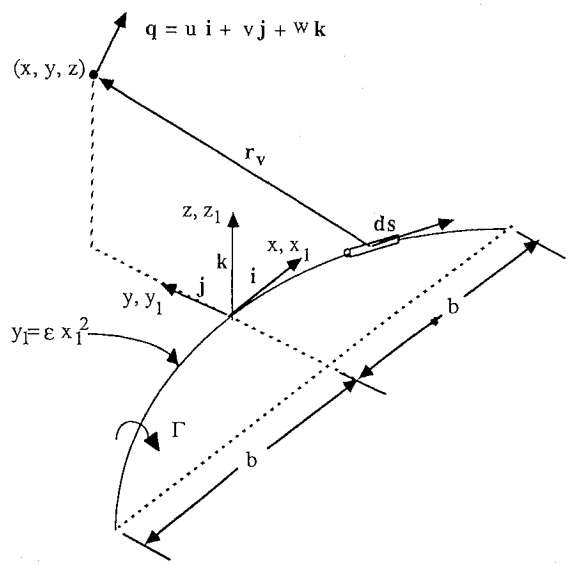

Fig. 4 Geometry for integration of the Biot-Savart law over a parabolic arc.

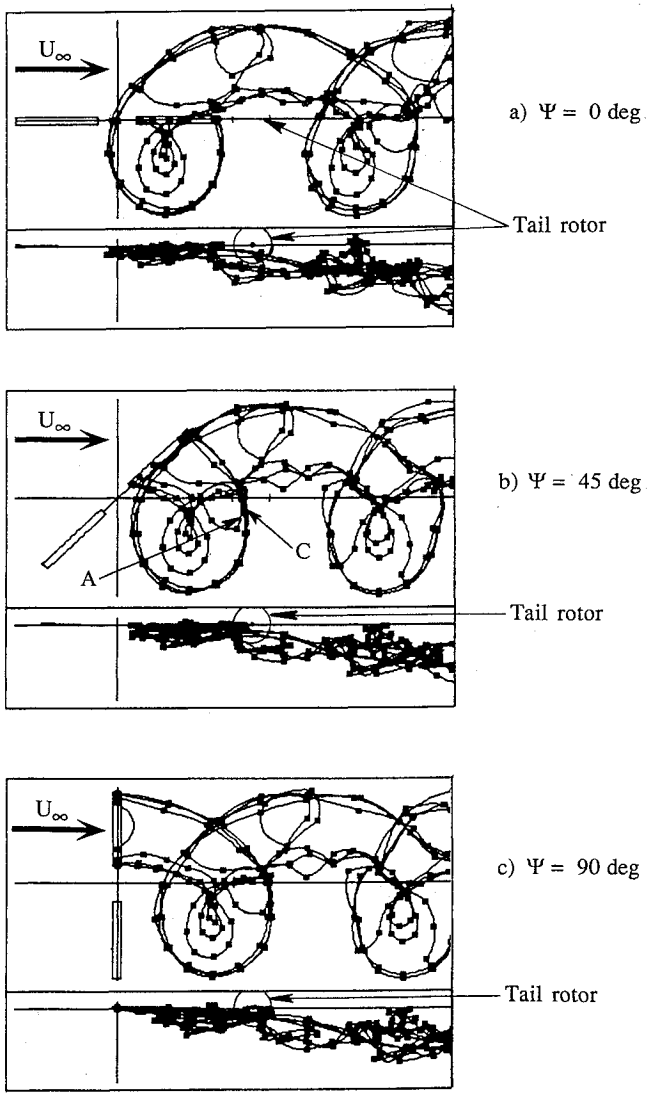

Fig. 5 Top and side views of the wake geometry of one blade and tail-rotor position for a two-bladed rotor at advance ratio 0.3 (Letters denote particular vortex intersection events.)

radius of curvature of the center of the parabola. The centered parabola extends from $-b<x<b$, where $\epsilon b = r/2\rho \ll 1$.

After extensive manipulation of the Biot-Savart integral, the following relatively simple result is obtained:

$$q_c = \frac{\Gamma}{4\pi}(-z\boldsymbol{j}+y\boldsymbol{k})(1-2\epsilon y)^{3/2}\left[\frac{2(1-2\epsilon y)}{y^2+z^2+r_c^2}-\frac{1}{b^2}\right]$$

$$+\frac{\Gamma}{4\pi}\epsilon\boldsymbol{k}(1-2\epsilon y)^{3/2}\left[-2+\ell n4+\ell n\left(\frac{b^2(1-2\epsilon y)}{y^2+z^2+r_c^2}\right)\right] \quad (3)$$

This result applies for the vortex arc having the actual physical core size r_c, hence the notation q_c for the velocity. The corresponding velocity for the fat core, denoted by q_f, is obtained simply changing the core size to r_f. The required analytical correction is the actual core velocity minus the fat core velocity, namely

$$\Delta q = q_c + q_f \quad (4)$$

Even with the application of the coordinate transformations required to complete the local adjustments, very little computational expense is incurred in the calculation of the velocity field at sufficient points in the tail-rotor plane to obtain very high spatial resolution. These calculations have also proven to be extremely accurate, as will be seen below.

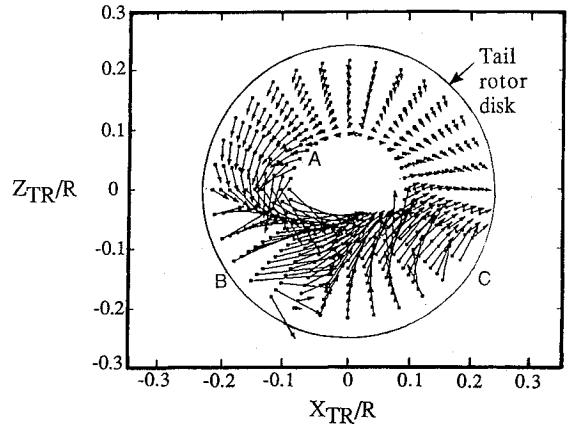

Fig. 6 Snapshot of wake-induced crossflow velocity in the tail-rotor disk corresponding to Fig. 5b. Tail-rotor hub at $X_{TR}=Z_{TR}=0$.

Examination of Typical Interactions and Solution of Model Problems

One objective of this effort was to investigate the type of interactions characteristic of typical helicopter flight conditions. The results shown in Ref. 12 include discussion of the impact of climb angle, tail-rotor inflow, and forward flight velocity. This section briefly reviews some of the results of the representative model problems discussed there that exercise the free-wake reconstruction program and the local velocity correction routine outlined in the previous section. The calculations involve various choices for the rotor configurations, the flight condition, the level of refinement in the wake model, the points in space at which the velocity field is to be surveyed, the size of the fat core, and the number of interpolated time steps. The results shown here are restricted to the case of two-bladed rotor at moderate forward speed in level flight, and features a wake models with eight filaments trailing from each blade. For these calculations the fat core was scaled to be from three to four times larger than the actual core size. The velocity calculations are carried out at points downstream of the main rotor, on or near the location of typical tail rotors on single-rotor helicopters. Temporal interpolation factors up to five have been used.

For the purpose of demonstrating the techniques developed here, it was judged appropriate to scrutinize a single representative case in detail. Thus, the discussion focuses on sample calculations of a "generic" two-bladed rotor at a thrust coefficient of 0.004 in level flight. The results shown here deal with a case at advance ratio 0.3, and with a tail rotor located $1.3R$ downstream of the main rotor (hub to hub distance) with a radius of $0.2R$. The tail-rotor hub is here assumed to be at the same vertical level as the main-rotor hub.

Principal Forms of Main-Rotor-Wake/Tail-Rotor Interactions

Figure 5 shows the wake configuration for one blade of this two-bladed rotor at three instants in time, while Fig. 6 shows a snapshot of the velocity at $\Psi = 45$ deg as the main-rotor vortices are convected through the tail-rotor disk. The swirling flow characteristic of the main-rotor vortices is evident, though it is necessary to cross reference these flow patterns with the views of the main-rotor wake shown in Fig. 5 to identify the particular vortices being swept through the tail-rotor disk (note: filaments with a counter-clockwise sense as seen from downstream of the blade are referred to as positive, while the opposite-sign filaments, usually trailed inboard, are termed negative). The dense cluster of positive filaments that form the tip vortex are evident in Fig. 5a; succeeding plots show these positive vortices being convected through the tail-rotor disk, along with the more highly distorted inboard filaments.

It should be remembered that the phrase "tail-rotor disk" for the present only implies a location downstream of the main

rotor; methods for explicit inclusion of the tail rotor and its wake are discussed in Ref. 12. In the absence of the inflow distortion caused by a tail rotor, the filament intersection angles are nearly constant as they pass through this region in the advance ratio 0.3 case. Also, the filaments that intersect the disk maintain close spacing in the z direction as they are convected through the tail-rotor region in this case.

Some insight into typical tail-rotor flowfields can be gathered through detailed examination of the velocity field on the tail-rotor disk. Crossflow plots such as Fig. 6 make the presence of intersecting vortices easy to discern, but the principal velocity component of interest in the prediction of blade loading is that normal to the tail-rotor disk. Figure 7 shows a contour plot of this normal component in the vicinity of the tail-rotor disk for one instant in time corresponding to Fig. 5b. Note that the location of steep gradients in normal velocity in Fig. 7 correspond to to the vortex intersections evident in Fig. 5b. (Each of the contour lines in Fig. 7 correspond to increments of 1.5% of freestream velocity; dotted lines indicate flow out of the page while solid lines reflect flow into the page.) The intersections denoted A and B reflect nearly perpendicular intersections of tip vortices with the disk, while C corresponds to a nearly parallel interaction of the disk with filaments trailed from the inboard part of the blade.

As a result of the initial comparisons made here and in Ref. 12, it was observed that the freestream convection largely determines the trajectory of both positive and negative vortices in high-speed cases, suggesting that the filaments will transit the disk along a relatively narrow, highly repeatable path. The intensity of the blade/vortex interactions that result, though, will depend not only on the intersection trajectories but on the relative phasing of the vortex motion and the tail rotor as well. As is discussed in more detail in Ref. 12, at lower speeds the high downwash along the wake centerline sweeps most discrete filaments away from the disk leaving only relatively few tip filaments that are trailed immediately upstream of the disk to undergo interactions with the tail rotor. For low as well as high speed, the positive tip vortices intersect the disk at angles very near 90 deg. The important role of these tip vortices is evident from Fig. 7, but the significant contributions of the inboard filaments should be noted as well.

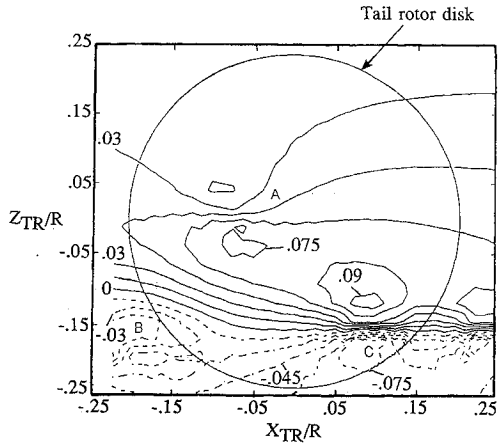

Fig. 7 Contour plot of velocity normal to the tail rotor disk corresponding to Fig. 5b. (See text for definitions of A, B, and C.)

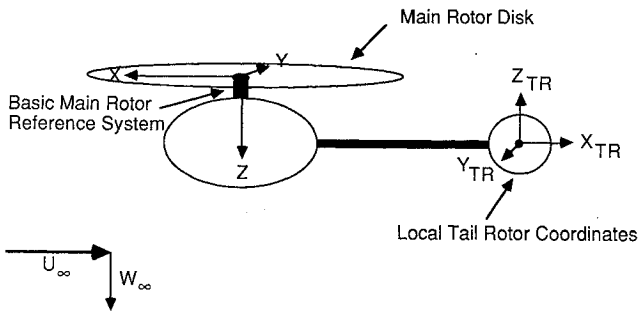

Fig. 8 Coordinate axes for main-rotor/tail-rotor interaction.

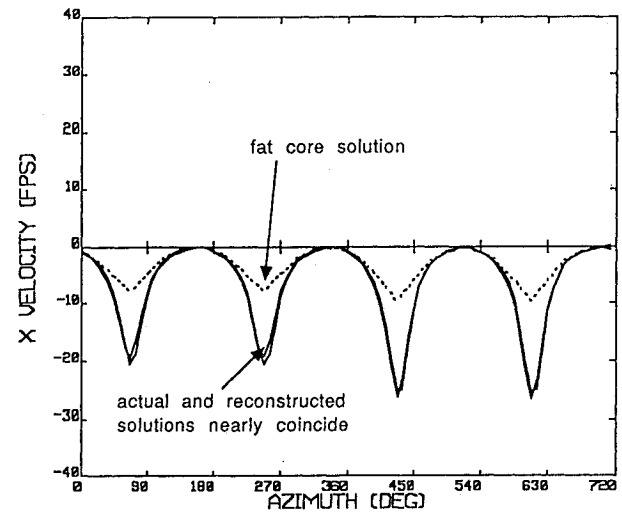

a) X component

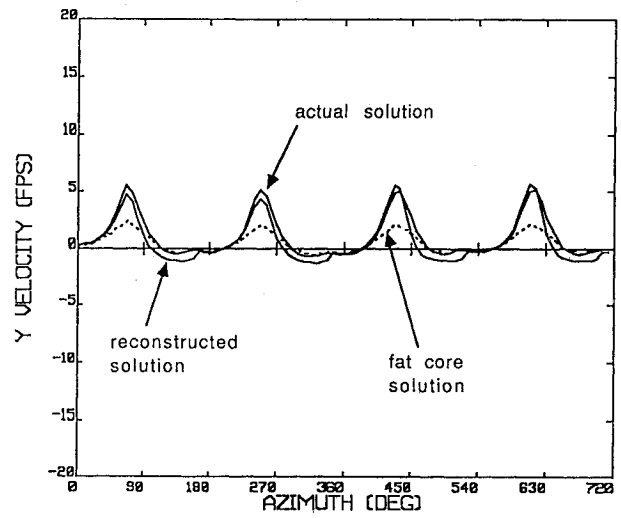

b) Y component

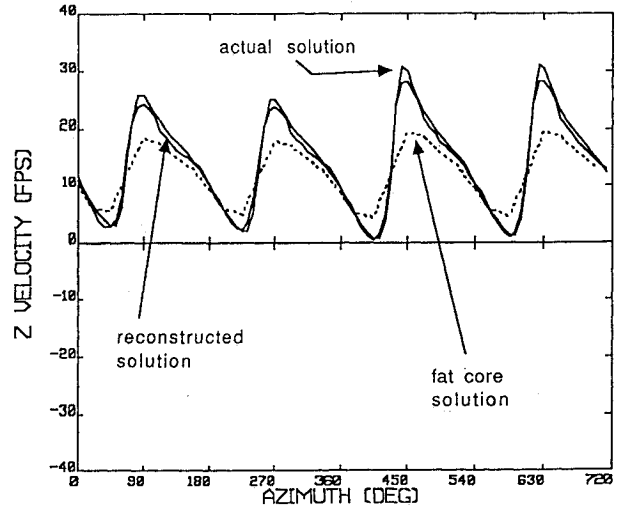

c) Z component

Fig. 9 Reconstruction of velocity at the tail-rotor hub using 3:1 time interpolation (16 steps interpolated to 48 steps per main-rotor revolution). (Two-bladed main rotor, $\mu = 0.3$, $C_T = 0.004$.)

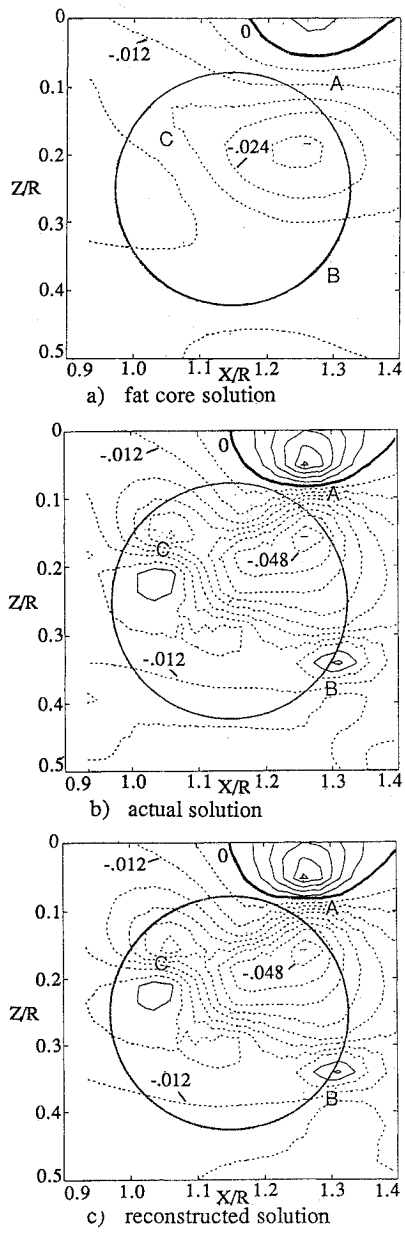

Fig. 10 Contour plots of U on the tail-rotor disk for $\mu = 0.14$, $C_T = 0.0042$. (Contours = $.006\Omega R$.)

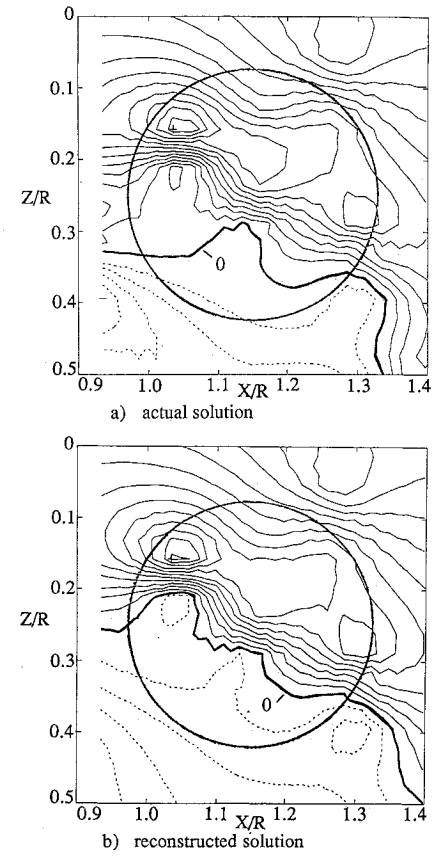

Fig. 11 Contour plots of V on the tail-rotor disk for $\mu = 0.14$, $C_T = 0.0042$. (Contours = $0.006\Omega R$.)

Sample Problems Using the Reconstruction Analysis

Several sample problems were undertaken to examine the ability of the reconstruction program to predict the velocity field downstream of the tail rotor using the fat core solution for the flowfield as a starting point. The first set considered made use of the two-bladed rotor described earlier operating at an advance ratio of 0.3 and a thrust coefficient of 0.004. The velocity field was sampled over a rectangular region centered 1.3R downstream of the and 0.2R below the main-rotor hub; this center point corresponds to the tail-rotor hub location on a typical single-rotor helicopter. The following results discussed show the time history of velocity at this hypothetical hub location for a case featuring the use of substantial time interpolation in conjunction with the core corrections. This case attempts to reconstruct the velocity field obtained at the hub using 48 time steps per (main) rotor revolution and the actual core from a relatively coarse solution featuring sixteen time steps per rev and a fat core. Note the reference frames for these calculations illustrated in Fig. 8.

Here the time step used for the free-wake solution with the fat core was three times larger than in the simulation with the actual core. Sixteen time steps per main-rotor revolution were used for the wake with the fat core, while 48 steps were used in the wake with the actual core. Also, the fat core used here had a radius three times that of the actual core. Figure 9 shows the result of interpolating the sixteen-step, fat core solution to recover the actual solution on the finer time scale. It is evident that the reconstructed solution is quite successful in recapturing the induced velocity at the tail-rotor hub over two periods of the revolution of the main rotor. Some of the velocity peaks are slightly underpredicted, but the correlation is, on the whole, quite good. This total calculation time for the solution with interpolation was approximately a factor of 27 below that of the noninterpolated case; as discussed earlier, the savings in computation time varies roughly as the cube of the temporal interpolation factor for initial value problems. Similar results were observed for a case with a five-to-one interpolation ratio, though again some underprediction of peak levels was observed.

These results deal only with a rotor in high-speed flight and focus on the time history of velocities at a single point in space, the rotor hub. To get a broader picture of the capabilities of the reconstruction program, a third sample problem was undertaken. Here, the flowfield over the entire planar region surrounding the tail-rotor disk was examined at an instant in time for the case of a Bell 222 rotor system in low-speed flight at advance ratio 0.14; this configuration features a two-bladed main rotor with the tail-rotor hub located located 1.15R downstream of and 0.22R below the main-rotor hub. The particular time "snapshot" was chosen to be representative of instances where significant interactions were taking place with the tail-rotor disk. The results shown in Figs. 10–12 are contour plots of all three velocity components at such an instant. In each of the contour plots, solid lines represent velocities that are in the positive coordinate direction, while dotted lines denote negative. (Note that the signs of the coordinates on the axes of the contour plots on the tail-rotor disk have been reversed as shown in Fig. 8, so that "up" on the helicopter is "up" on the page, while "aft" or "down-

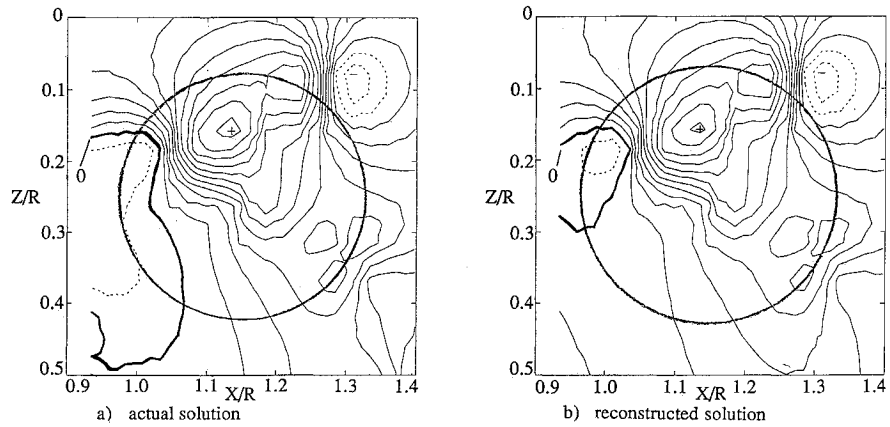

Fig. 12 Contour plots of W on the tail-rotor disk for $\mu = 0.14$, $C_T = 0.0042$. (Contours = $0.006\Omega R$.)

stream" is to the right.) The magnitude of the contour increments vary from plot to plot, and they are labeled accordingly. Three significant interactions are taking place: 1) a cluster of tip vortices, labeled A, intersecting the disk at very nearly normal incidence, each having an "age" of roughly 90 deg, i.e., they trailed from the generating blade one quarter of a rotor revolution previously; 2) a single root filament, labeled B, roughly 450-deg "old", intersecting at an angle of 30 deg off the normal; and 3) a cluster of four inboard vortices, labeled C, about 270-deg old, intersecting at angles varying from 20 to 40 deg off normal.

First, Fig. 10a shows the contour plot for the initial free-wake run with the fat core (three times the size of the actual core) in place, displaying the U velocity. The relatively wide spacing of the contour lines (each of which represents 5 fps or $0.006\Omega R$ of velocity increment) reflects the smooth flow gradients associated with the fat core solution. Next, Fig. 10b shows the contour plot of the same velocity component with the nominal vortex core of $0.03R$; note that the contour lines are much more densely spaced than in Fig. 10a, which is indicative of the steep velocity gradients imposed by using the relatively small actual core. Finally, Fig. 10c shows the velocity contours over the same area after the reconstruction program has been invoked. It is evident that the reconstruction routine has been very successful in capturing the behavior predicted using the actual core.

Similar results were also generated for the V and W velocity components, and the comparisons of the actual and reconstructed results are shown in Figs. 11 and 12. Those results produce additional evidence of the ability of this routine to reconstruct the actual core solution using local flow corrections.

Summary and Recommendations for Future Work

The principal objective of this effort was to demonstrate the feasibility of implementing an efficient and accurate calculation scheme for velocities induced at the tail rotor by the main-rotor wake. The results discussed here have demonstrated the success of a new approach to the efficient calculation of high-resolution velocity fields in vortex-dominated flows. This new approach takes advantage of the fact that the steep spatial velocity gradients that contribute to tail rotor noise are local phenomena, which can be captured by applying correction terms to the low-resolution background flow generated by simple, relatively efficient free-wake calculations. Representative sample calculations have shown that accurate time histories of wake-induced velocities can be reconstructed while using one to two orders of magnitude less CPU time than full Lagrangian free-wake calculations. In addition, high-fidelity reconstructions of instantaneous spatial velocity distributions were obtained from initially coarse wake models by applying these local correction terms. The combined evidence of these results indicate that main-rotor/tail-rotor interaction calculations featuring the high level of temporal resolution required for acoustic calculations are now within reach, and that the full-span main-rotor wake model used in previous work can be successfully incorporated in such calculations.

Analysis of typical main-rotor/tail-rotor interactions indicated that the primary type of interaction characteristic of single-rotor helicopter is the near-normal intersection of relatively "young" tip vortices trailed from the main-rotor blades just upstream of the tail-rotor disk. In addition, typical plots of the wake geometry (e.g., Figs. 1 and 5) suggest that the inboard wake could impinge on the tail rotor in many flight conditions, particularly at high forward speed. Plots of the velocity field in and around the tail-rotor disk (such as Figs. 6 and 7) also suggest that this portion of the wake can make significant contributions to the local flowfield around the tail rotor, particularly the component normal to the disk. Future efforts must carefully consider the role of the inboard wake and how it can best be modeled.

In summary, this effort has provided several of the building blocks from which a general aeroacoustic analysis of main-rotor/tail-rotor interaction may be constructed. With regard to future efforts, it should be emphasized that though the current work has focused on the prediction of tail-rotor flowfields these same techniques can be generalized to handle any type of rotor-wake/rotor interaction, including the interaction of the main rotor with its own wake. Several tentative conclusions have been drawn about the preferred approach in developing such general analyses. In the main-rotor/tail-rotor case, each rotor could be modeled using the full-span wake model, though the main-rotor inflow could in general be considered as a "frozen" or predetermined input to the tail-rotor simulation. Thus, it is possible that the refined flowfield definition made possible by the use of full-span wakes of curved vortex elements could be retained without the computational expense of two fully coupled free-wake calculations. The desirability of this approach could be tested with sample comparisons using fully coupled calculations as a benchmark.

In addition to this modification of the wake model, new efforts should be undertaken to refine and extend the underlying physical models. To provide accurate definition of unsteady aerodynamic loads due to vortex wake interactions, appropriately modified versions of existing airfoil transfer functions should be used to account for these unsteady loads. Also, a major effort should be made to introduce physically realistic vortex core models, so that the velocity field experienced by lifting surfaces interacting with the vortex wake will be correctly handled. In addition, the potentially important contributions of fuselage or empennage surfaces should be considered and correlation efforts undertaken with recent experimental efforts such as Ref. 18. Finally, another important consideration in follow-on work should be to take maximum advantage of the work done to date in the study of the acoustic output of aerodynamically loaded surfaces. Since the principal technical focus of the effort outlined here has been on sup-

porting the calculation of aerodynamic forces on isolated rotors for aeroacoustics applicants, an existing acoustic propagation model such as NASA's WOPWOP (Refs. 19 and 20) should be incorporated into the simulation to provide the capability of predicting the noise of interacting rotors. An aerodynamic loads program based on the techniques developed here and incorporating these extensions and modifications should provide a suitable foundation for a general analysis of rotor-wake/rotor interaction noise.

Acknowledgment

This research was supported by Contract NAS1-18607 from NASA Langley Research Center. The technical monitor was J. C. Hardin.

References

[1] Leverton, J. W., Pollard, J. S., and Willis, C. R., "Main Rotor-Wake/Tail Rotor Interactions," *Vertica*, Vol. 1, No. 3, 1977, pp. 213–222.

[2]Ahmadi, A. R., "An Experimental Investigation of Blade Vortex Interaction at Normal Incidence," *Journal of Aircraft*, Vol. 23, No. 1, 1986, pp. 47–54.

[3]Jacobs, E. W., and Shenoy, R. K., "Acoustic Characteristics of Tail Rotors of the Effects of Empennage Interactions," *Proceedings of the 43rd Annual Forum of the American Helicopter Society*, American Helicopter Society, Alexandria, VA, 1987, pp. 437–451.

[4]Schlinker, R. H., and Amiet, R. K., "Rotor Vortex Interaction Noise," NASA CR-3744, Oct. 1983.

[5]Edwards, B. D., Peryea, M. A., and Brieger, J. T., "1/5th Scale Model Studies of Main Rotor and Tail Rotor Interactions," *Proceedings of the American Helicopter Society National Specialist' Meeting on Aerodynamics and Aeroacoustics*, American Helicopter Society, Alexandria, VA, 1987.

[6]Tadghighi, H., "An Analytical Model for Prediction of Main Rotor/Tail Rotor Interaction Noise," Paper A-88-44-70-D000, 44th Annual Forum of the American Helicopter Society, American Helicopter Society, Alexandria, VA, 1988.

[7]Bliss, D. B., Quackenbush, T. R., and Bilanin, A. J., "A New Methodology for Helicopter Free Wake Analyses," Paper A-83-39-75-000, 39th Annual Forum of the American Helicopter Society, American Helicopter Society, Alexandria, VA, 1983.

[8]Bliss, D. B., Teske, M. E., and Quackenbush, T. R., "A New Methodology for Free Wake Analysis Using Curved Vortex Elements," NASA CR 3958, July 1987.

[9]Bliss, D. B., Dadone, L. U., and Wachspress, D. A., "Rotor Wake Modeling for High Speed Applications," *Proceedings of the 43rd Annual Forum of the American Helicopter Society*, American Helicopter Society, Alexandria, VA, 1987, pp. 17–33.

[10]Quackenbush, T. R., Bliss, D. B., and Wachspress, D. A., "Preliminary Development of an Advanced Free Wake Analysis for Rotor Unsteady Airloads," Continuum Dynamics, Inc., Rept. 87-06, NASA Contract NAS2-12554, Aug. 1987.

[11]Quackenbush, T. R., Bliss, D. B., Wachpress, D. A., and McKillip, R. M.,"Free Wake Analysis of Rotor Configurations for Reduced Vibratory Airloads," *Proceedings of the American Helicopter Society's National Specialists' Meeting on Rotorcraft Dynamics*, American Helicopter Society, Alexandria, VA, 1989.

[12]Quackenbush, T. R., Bliss, D. B., and Bilanin, A. J., "Prediction of High Resolution Flow Fields for Tail Rotor Aeroacoustics," Continuum Dynamics, Inc., Final Rept. 88-08, NASA NAS1-18607, August 1988.

[13]Landgrebe, A. J., "An Analytical and Experimental Investigation of Helicopter Rotor Hover Performance and Wake Geometry Characteristics," U.S. Army Air Mobility Research and Development Laboratory TR-71-24, June 1971.

[14]Scully, M. P., "Computational of Helicopter Rotor Wake Geometry and Its Influence on Rotor Harmonic Airloads," MIT ASRL TR 178-1, Massachusetts Inst. of Technology, Cambridge, MA, March 1975.

[15]Egolf, T. A., and Landgrebe, A. J., "Helicopter Rotor Wake Geometry and Its Influence in Forward Flight," Vols. I and II, NASA CR-3726 and 3727, Oct. 1983.

[16]Martin, R. M., and Hardin, J. C., "The Spectral Characteristics of Rotor Blade-Vortex Interaction Noise," AIAA Paper 87-0251, Jan. 1987.

[17]Quackenbush, T. R., and Bliss, D. B., "Free Wake Flow Field Calculations For Rotorcraft Interactional Aerodynamics," *Vertica*, Vol. 14, No. 3, 1990, pp. 313–327.

[18]Ellin, A. D. S., "Flight Measurements Indicating Key Features of Tail Rotor Loading Distribution," *Proceedings of the RAE/AHS Meeting on Helicopter Yaw Control*, American Helicopter Society, Alexandria, VA, 1990.

[19]Brenter, K. S., "Prediction of the Helicopter Rotor Discrete Frequency Noise,"NASA TM 87721, Oct. 1986.

[20]Quackenbush, T. R., Bliss, D. B., and Mahajan, A. J., "High Resolution Flow Field prediction for Tail Rotor Aeroacoustics," *Proceedings of the 45th Annual Forum of the American Helicopter Society*, American Helicopter Society, Alexandria, VA, 1989, pp. 99–114.